ISSN 0016-8521, Geotectonics, 2022, Vol. 56, No. 6, pp. 791–809. © Pleiades Publishing, Inc., 2022.
ISSN 0016-8521, Geotectonics, 2022. © Pleiades Publishing, Inc., 2022.

Golpayegan Metamorphic Complex (Sanandaj–Sirjan Zone, Iran) as Evidence for Cadomian Back-Arc Magmatism: Structure, Geochemistry and Isotopic Data

S. Ahmadi-Bonakdar[a], S. M. Tabatabaei Manesh[a, *], A. Nadimi[a], A. Mirlohi[a], J. F. Santos[b], and O. V. Parfenova[c]

[a] *University of Isfahan, Department of Geology, Hezarjrib, Isfahan, 81746-73441 Iran*
[b] *University of Aveiro, Department of Geosciences, Geobiotec, Aveiro, 3810-193 Portugal*
[c] *Lomonosov Moscow State University, Geology Faculty, Department of Petrology, Moscow, Russia*
**e-mail: tabatabai@sci.ui.ac.ir*

Received July 4, 2022; revised October 3, 2022; accepted November 7, 2022

Abstract—The Golpayegan metamorphic complex is located in the Sanandaj-Sirjan Zone, Iran. This complex consists of various metamorphic rocks including schists, marbles, slates, gneisses, and amphibolites, most of them have Neoproterozoic age. The presence of structures such as sigma fabrics, boudinage, folded boudinage and interfering fold patterns indicates the occurrence of more than two deformation phases in the Golpayegan metamorphic complex. The measurement of strain intensity in the folds indicated deep immersion of structures and old Precambrian settings that had been influenced by orogenic events in the Neoproterozoic. These deformed rocks were exposed during extensional movements and, subsequently, sheared. The results based on field works shown geochemical relations and initial εNd(600 Ma) values of amphibolites in three sampling points located in Golpayegan region manifested that the protolith of the first (*a*') and second (*b*') sampling points had mantle origin (ortho-amphibolite), whilst protolith of the third (*c*') sampling point had sedimentary origin (para-amphibolite). Geochemically, the Golpayegan ortho-amphibolites showed subalkaline basalt-basaltic andesite compositions of tholeiitic affinity. The negative anomalies of Nb and Ti relative to Pb, La, and Ce in the primitive mantle-normalized spider-diagram and εNd(600 Ma) values revealed the subduction environment for ortho-amphibolites. The ortho-amphibolites exhibited the intermediate chemistry between the normal mid-ocean ridge basalt and island-arc tholeiitic basalt. Enrichment in large ion lithophile elements (LILE), light rare earth elements (LREE), and relative depletion in high field strength elements (HFSE) suggest the back-arc basin setting for the Golpayegan ortho-amphibolites. The primitive magma of the ortho-amphibolites was produced by 8–20% melting of spinel lherzolite. According to the Neoproterozoic age of the Golpayegan ortho-amphibolites and their relationship with the Golpayegan granitic gneiss (596–578 Ma), it shows that they can be related to the Cadomian back-arc basin in the north of Peri-Gondwana at the Neoproterozoic. The high values of $^{87}Sr/^{86}Sr$ (0.708450–0.714986) interpreted as result of seawater hydrothermal alteration.

Keywords: amphibolite, deformation, Cadomian back-arc, Golpayegan, Sanandaj–Sirjan Zone, Iran
DOI: 10.1134/S0016852122060024

INTRODUCTION

The Zagros orogenic belt is portion of the Alpine–Himalayan orogenic belt was formed during the convergence between the Arabian and Eurasian plates and includes the Urumieh–Dokhtar magmatic arc, metamorphic and magmatic Sanandaj–Sirjan zone (SSZ), and Zagros fold-thrust belt [1, 7] (Fig. 1a). The Golpayegan area is located in the SSZ and northern margin of the Zagros orogenic belt. In the area, Golpayegan metamorphic complex (GMC) was known as a complex and portion of the Precambrian continental basement [66]. Most of the Iranian basements area comprised of the Cadomian igneous and metamorphic rocks [57].

Defining the age of Golpayegan amphibolites using K–Ar isotopic technique of 180–150 Ma (Middle-Upper Jurassic) suggested cooling process of the metamorphic rocks [9, 49]. The xenocrystic zircons placed in the amphibolites of the Muteh–Golpayegan metamorphic complex may be derived from the Archean basement which lacked exposure [59]. There was suggested the age of 596–578 Ma of the Golpayegan–Muteh granite using U–Pb method [23].

The Precambrian rocks and occurrence of multiple deformations of different characteristics and intensities in the Sanandaj–Sirjan area, indicated deep and old Precambrian setting in the area [39]. The Ediacaran–Cambrian arc-type magmatism (so-called Cado-

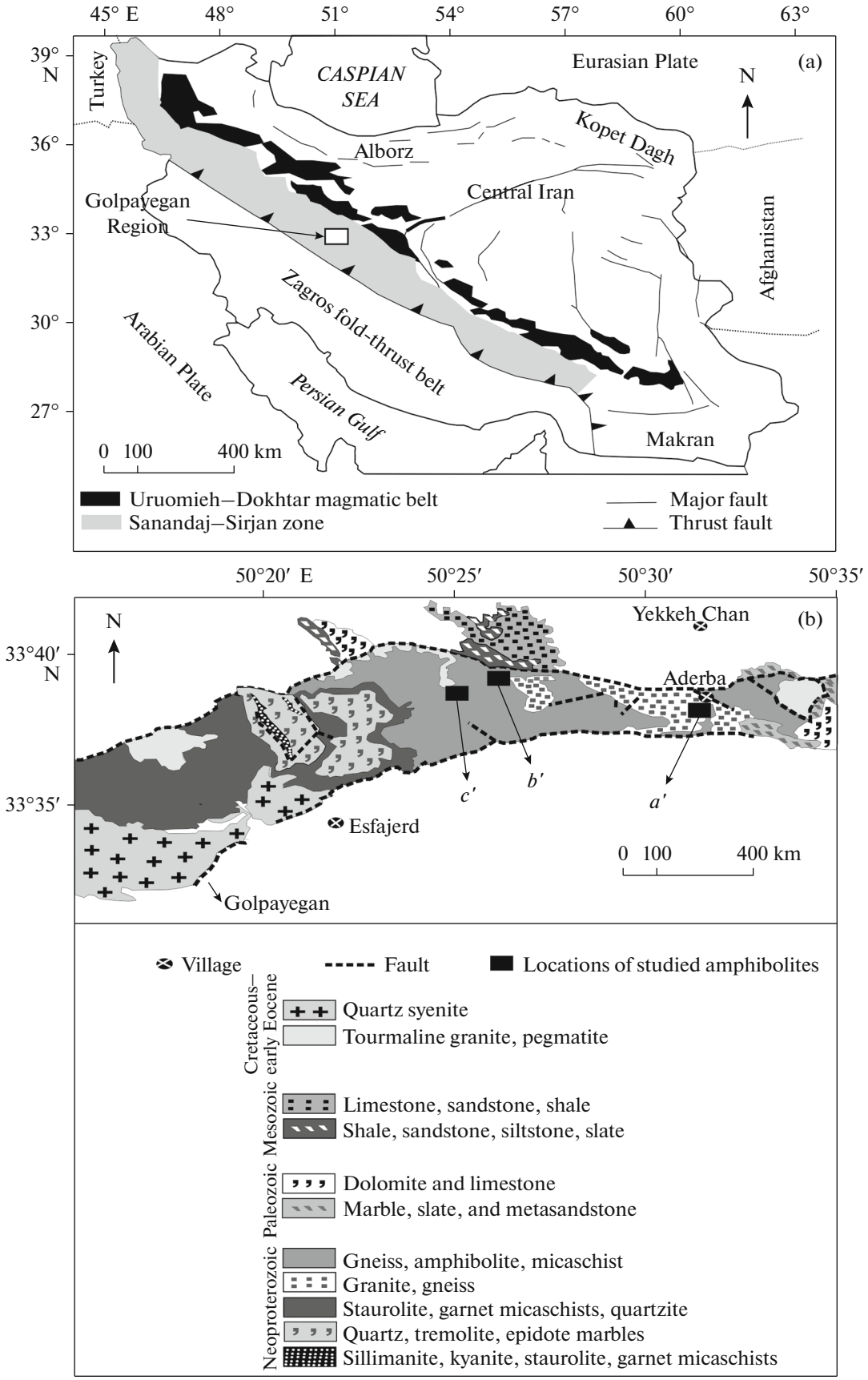
45° E
48°
51°
54°
57°
60°
63°
39° N
36°
33°
30°
27°
Turkey
CASPIAN SEA
Eurasian Plate
(a)
N
Kopet Dagh
Alborz
Central Iran
Golpayegan Region
Afghanistan
Zagros fold-thrust belt
Arabian Plate
Persian Gulf
Makran
0 100 400 km
Uruomieh–Dokhtar magmatic belt
Sanandaj–Sirjan zone
Major fault
Thrust fault
50°20′ E
50°25′
50°30′
50°35′
33°40′ N
33°35′
N
Yekkeh Chan
(b)
Aderba
c′
b′
a′
Esfajerd
0 100 400 km
Golpayegan
Village
Fault
Locations of studied amphibolites
Cretaceous–early Eocene
Quartz syenite
Tourmaline granite, pegmatite
Mesozoic
Limestone, sandstone, shale
Shale, sandstone, siltstone, slate
Paleozoic
Dolomite and limestone
Marble, slate, and metasandstone
Neoproterozoic
Gneiss, amphibolite, micaschist
Granite, gneiss
Staurolite, garnet micaschists, quartzite
Quartz, tremolite, epidote marbles
Sillimanite, kyanite, staurolite, garnet micaschists

Fig. 1. The major structural units of Iran (after [18], modified) the location of Golpayegan metamorphic complex in Sanandaj–Sirjan zone. The sampling points *a*', *b*' and *c*' of amphibolite are shown in black squares (a); Geological map of rock units of the Golpayegan metamorphic complex (after [37], modified) (b).

mian arc) along the northern margin of Gondwanan supercontinent generated from Late Neoproterozoic to Early Paleozoic (600–500 Ma) blocks within the orogenic belt [21, 31, 56]. The Proto-Tethys Ocean surrounded Gondwana from North Africa to Australia in the Late Proterozoic to the Early Paleozoic [64].

The Proto-Tethys Ocean subducted beneath the northern edge of the Peri-Gondwana during ~600 Ma (Late Precambrian) giving rise to the Cadomian arc. Following that subduction, rifting occurred at the northern margin of the Gondwana supercontinent which was drufting to the north. The rifting also led to the thinning of the crust, triggering igneous activity (between 590–540 Ma) in the northern most parts of Gondwana [5, 21]. Rifting of the most of the northern margin of Gondwana during the Permian (250–280 Ma) and the expansion of the Neo-Tethys Ocean are responsible for separation of Central Iran, SSZ, Alborz (Iran), and Tauride–Anatolian (Turkey) blocks and moving towards Eurasia, each block contained Cadomian rocks [69]. These terranes again re-amalgamated to the Arabian Plate during the Oligo-Miocene times [56]. The Cadomian magmatism is seen in various regions of Iran, Turkey, Europe, and Tibet [5, 21, 31, 57, 71].

The goal of this study is to adduce the Cadomian arc magmatism event in the Golpayegan metamorphic complex (GMC) based on evidence of deformation in metamorphic rocks (e.g., the examination of fold interference patterns) as well as to determine the petrological and geochemical nature and geotectonic setting of the Golpayegan amphibolites.

GEOLOGICAL SETTING

The Sinandaj–Sirjan zone (SSZ), as one of the main basement blocks of Iran, is located between the northwestern margin of the Arabian Plate and the micro-continent of Central-Eastern Iran [7, 10, 62, 65]. The Sinandaj–Sirjan zone extends ~1500 km from the northwest (Sanandaj) to southeast (Sirjan) parallel to the Zagros fold-thrust belt with width of 150–200 km (Fig. 1a) [67]. Tectonically, the Sinandaj–Sirjan zone is one of the most active zones of Iran due to specific metamorphic processes and is distinct from other parts of the geological divisions of Iran [18, 26].

The Sinandaj–Sirjan zone consists of metamorphic, igneous, and sedimentary rocks of late Neoproterozoic to Neogene age in the hanging wall of the Main Zagros Thrust [1, 36]. Also, it is a region of multistage deformation and metamorphism phases that occurred under greenschist and amphibolite facies [36].

The Sinandaj–Sirjan zone (SSZ) is considered to be the continental active margin of Neo-Tethys. The Neo-Tethys opened and closed along the southwest margin of the SSZ, whilst the Paleo-Tethyan lied to the north of Sinandaj–Sirjan zone [7, 55]. There are significant similarities between Sinandaj–Sirjan zone and tectonic structures of the Central Iran in respect of magmatism, metamorphism, and orogenic events [9].

The Golpayegan metamorphic complex, as the study area is located at the NE margin of the central part of Sinandaj–Sirjan zone (Fig. 1a).

There are two fault systems in the study area that consists of:

— NW–SE trending faults striking parallel to the Zagros orogenic structures;

— NE–SW trending faults perpendicular to the first system that was formed during lateral extension movement after the Middle Miocene.

At this step, some NE–SW trending horsts and grabens were developed, and at the horsts, the Precambrian basement rock units were exposed [41].

Rock assemblages in the study area can be divided into the metamorphosed core and the non-metamorphosed cover. The core rocks are tectonically overlain by non-metamorphosed strata containing the Permian, Jurassic, Cretaceous, and Eocene sedimentary successions. The metamorphic core is mainly composed of schists, marbles, slates, gneisses and amphibolites, most of them have the Neoproterozoic age [37, 60] (Fig. 1b). Precambrian rocks include sillimanite-kyanite-staurolite-garnet-micaschist and quartz-tremolite-epidote-marble in the lower part and staurolite-garnet-micaschist, quartzite and gneiss, amphibolite, micaschist and granite gneiss in the upper part [37] (Fig. 1b).

ANALYTICAL METHODS

In this study, significant features of the folds, such as the orientation of axial surface, axis of the folds and the identification of different generations of folds, are amongst the important issues that were pondered in the structural studies of folds in Golpayegan region. Structurally examine a fold is confined to the size of the folded units. In Golpayegan region, several deformation phases can be seen in which the differing phases of deformation range from ductile to ductile-brittle.

The amount of strain was statistically measured as the amount of shortening in the folds (Table 1).

Mineral chemical analyses were conducted by the wave-length-dispersive electron probe microanalyzer (EPMA) JEOL JXA-8800 (WDS) (Jeol, Ltd., Tokyo, Japan) at the Moscow State University (Moscow, Russia). The studies were performed under an accelerating voltage of 20 kV and the beam current of 12 nA.

Table 1. The results of strain measurements of 21 fold samples in the surveyed cherty marbles and banded gneisses in GMC

Number	L_1	L_2	e	Shortening, %	S	Deformation intensity
1	20	4.3	–0.78	78	0.21	H-I
2	19	9	–0.52	52	0.47	I
3	15.3	2.8	–0.81	81	0.18	H-I
4	25	3.7	–0.85	85	0.14	H-I
5	10	1.8	–0.82	82	0.18	H-I
6	11	6.2	–0.43	43	0.56	M
7	37.8	11.1	–0.70	70	0.29	H-I
8	13	4.7	–0.63	63	0.36	I
9	6.5	1.6	–0.75	75	0.24	H-I
10	12	3.6	–0.70	70	0.30	I
11	8.9	3.7	–0.58	58	0.41	I
12	19.7	4.9	–0.75	75	0.24	H-I
13	12.4	2.8	–0.77	77	0.22	H-I
14	7	1.5	–0.78	78	0.21	H-I
15	7.7	2.4	–0.68	68	0.31	I
16	14.7	5.2	–0.64	64	0.35	I
17	16.6	5.9	–0.64	64	0.35	I
18	11.7	5.4	–0.53	53	0.46	I
19	6.1	3.4	–0.44	44	0.55	M
20	18.2	5.8	–0.68	68	0.31	I
21	44.5	14.6	–0.67	67	0.32	I

L_1 (primary length); L_2 (secondary length); $e = (L_2 - L_1)/L_1$; $S = L_2/L_1$; M (moderate deformation); I (severe deformation) and HI (very intense deformation).

To implement the thermometry studies using coupled minerals of hornblende-plagioclase, equilibrium between them and absence of reaction rim on the petrographic studies appear to be a desideratum, which has been taken into account in choosing decent samples for EPMA analysis.

The structural formula and Fe^{2+} and Fe^{3+} contents of amphiboles were calculated after Schumacher [54]. Tables 2 and 3 include the results of chemical studies of amphibole and plagioclase.

The whole-rock, major and trace-element compositions were determined using the Inductively Coupled Plasma–Mass Spectrometry (ICP–MS) at the Zarazma Mineral Studies Company, Ltd. (Tehran, Iran). Geochemical analyses of the Golpayegan amphibolites are shown in Table 4. In mineral analyses, mineral abbreviations are from Whitney and Evans [74].

Sr–Nd isotopic compositions were measured at the Laboratory of Isotope Geology of the University of Aveiro (Portugal). The selected samples for Sr–Nd isotopic analysis were dissolved by HF/HNO_3 solution in poly-tetra-fluor-ethene (PTFE) Parr acid digestion bombs at a temperature of 200°C for three days. After evaporation of the final solution, the samples were dissolved in HCl (6.2 N), and then in acid digestion bombs. Also, they dried again.

The elements to analyze were purified by conventional ion chromatography technique in two stages: separation of Sr and REE in ion exchange columns containing AG8 50 W Bio-Rad cation exchange resin (i) followed by separation of Nd from other lanthanides in columns containing Ln Resin (Elchrom Technologies) cation exchange resin (ii).

All reagents used in the preparation of the samples were sub-boiling distilled, and the water was produced by a Milli-Q Element (Millipore) apparatus. The Sr was loaded on the single Ta filament with H_3PO_4, whiles Nd was loaded on Ta outer side filament with HCl in the triple filament arrangement. $^{87}Sr/^{86}Sr$ and $^{143}Nd/^{144}Nd$ isotopic ratios were defined using multi-collector Thermal Ionization Mass Spectrometer (TIMS) VG Sector-54. Data were acquired in the dynamic model with peak measurements at 1–2 V for ^{88}Sr and 0.5–1.0 V for ^{144}Nd. The Sr–Nd isotopic ratios were corrected for mass fractionation relative to $^{88}Sr/^{86}Sr = 0.1194$ and $^{146}Nd/^{144}Nd = 0.7219$.

The SRM-987 standard gave an average value of $^{87}Sr/^{86}Sr = 0.710265(19)$ ($N = 11$; conf. lim = 95%) and JNdi-1 standard gave an average value of

Table 2. Chemical analyses (in wt %) and calculated structural formula of amphiboles of the Golpayegan amphibolites in the GMC

Components	*c*'-location		*b*'-location		*c*'-location	
	hb32-430	hb31-430	hb12-447	hb11-447	hb3-3-323	hb2-4-323
SiO_2	47.83	45.16	44.81	47.15	44.57	44.51
Al_2O_3	8.34	11	12.34	9.98	12.27	11.55
MgO	13.98	12.51	11.45	13.09	9.75	9.63
FeO	13.05	14.05	16.59	18.63	17.12	17.26
TiO_2	0.51	0.83	0.54	0.49	0.92	0.98
MnO	0.23	0.25	0.4	0.54	0.3	0.34
CaO	11.5	11.23	10.51	7.87	11.55	11.49
Na_2O	1.06	1.41	1.41	1.14	1.26	1.35
K_2O	0.16	0.28	0.2	0.2	0.53	0.49
Total	96.66	96.72	98.24	99.08	98.4	97.72
Oxygen#	23	23	23	23	23	23
Si	7.02	6.69	6.59	6.87	6.59	6.64
Al	1.44	1.92	2.14	1.71	2.14	2.03
Mg	3.06	2.76	2.51	2.84	2.15	2.14
Fe^{+2}	1.48	1.61	1.81	2.08	2.04	1.64
Fe^{+3}	0.11	0.11	0.19	0.15	0.06	0.49
Ti	0.05	0.09	0.06	0.05	0.10	0.11
Mn	0.03	0.03	0.05	0.06	0.04	0.04
Ca	1.81	1.78	1.65	1.23	1.83	1.84
Na	0.30	0.40	0.40	0.32	0.36	0.39
K	0.030	0.05	0.04	0.04	0.10	0.09
Al^{IV}	0.97	1.31	1.40	1.13	1.40	1.35
Al^{VI}	0.47	0.61	0.73	0.58	0.74	0.68
$Mg/(Mg + Fe^{+2})$	0.65	0.61	0.55	0.55	0.50	0.49
$Fe^{+2}/(Mg + Fe^{+2})$	0.34	0.38	0.45	0.44	0.49	0.50
$^{B}(Ca + {}^{B}\sum M^{2+})/\sum B \geq 0.75$	1	1	1	1	1.05	1.03
$^{B}Ca/^{B}(Ca + Na) \geq 0.75$	1	1	1	1	0.98	0.97
$^{c}(Al + Fe^{+3} + 2Ti)$	0.69	0.91	1.0458	0.84	1.01	1.39
$^{A}(Na + K + 2Ca)$	0.36	0.47	0.4821	0.38	0.43	0.43
Name	Magnesio-hornblende	Magnesio-hornblende	Magnesio-hornblende	Magnesio-hornblende	Magnesio-hornblende	Magnesio-hornblende

$^{143}Nd/^{144}Nd = 0.5120958(88)$ ($N = 12$; conf. lim = 95%, 2σ), during this study. The Rb–Sr and Sm–Nd isotope compositions are listed in Table 5.

RESULTS

Deformations of the Golpayegan Metamorphic Complex

The Golpayegan metamorphic complex has fold and boudin structures, which suggests the occurrence of several stages of deformation. Folds are a fundamental structure of contractional orogens, and yet deciphering their kinematic history continues to be controversial [20].

The folds' amplitude range from a few centimeters to a few meters in size (Fig. 2). Different phases of deformation have created differing patterns of folding in the study area (Fig. 2a). Superposed folds or interfering fold patterns are witnessed in Golpayegan region (Fig. 2b). In orogenic areas such as the study area at the Sanandaj–Sirjan Zone, interfering fold patterns are formed [51]. Superposed folds or fold interference patterns occur when one generation of folds is overprinted by a later generation [16, 50].

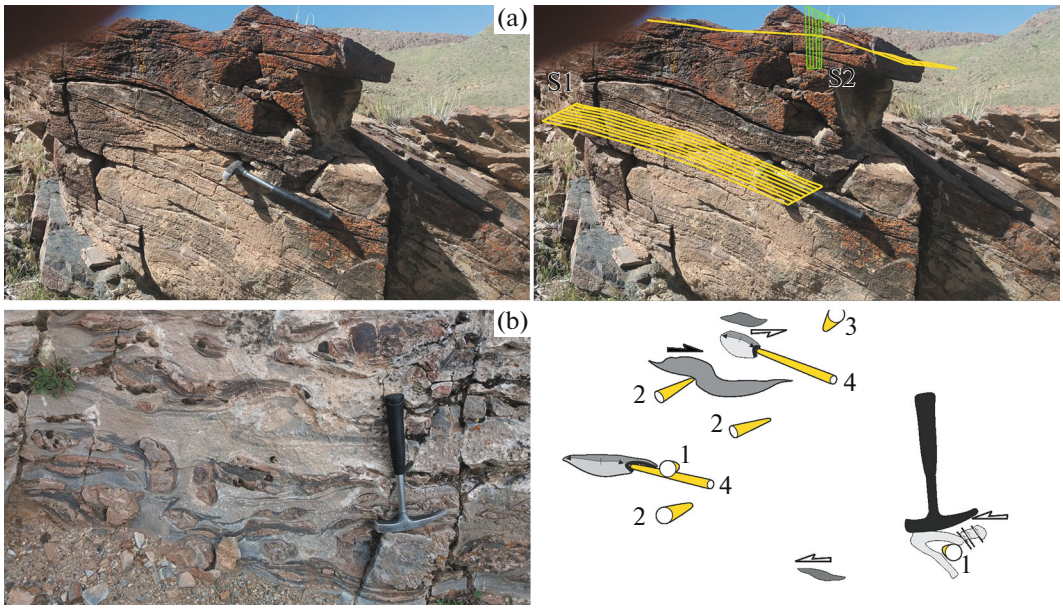

Fig. 2. Position of two axial planes, which implies two phases of deformation. The older fold (recumbent) of axial plane is marked in yellow and the newer fold is marked in green (a); patterns of interference (superimposed) folds, sigma fabric, boudinage, and folded boudinage. The axial planes are marked and numbered, in which identical numbers are presumably related to the certain deformation phase. Signatures of right- and left-lateral shear movements can be seen in this figure (b).

In Golpayegan region, the pattern of axes in folds is scattered in different directions, which indicates several phases of deformation (Fig. 2). Structural variety of the folds is one of the most important factors in the complexity of this region. The change of the folds' geometric elements at short distances indicates the influence of multiple stages of evolution on these rocks, connoting long and eclectic history.

Table 3. Chemical analyses (in wt %) and calculated structural formula of plagioclase of the Golpayegan amphibolites in the GMC

Components	*c*'-location		*b*'-location		*a*'-location	
	pl38-430	pl37-430	pl24-447	pl23-447	Pl2-323	Pl3-323
SiO_2	57.85	56.77	57.89	60.34	59.86	57.9
Al_2O_3	26.48	26.89	26.9	25.17	26.95	28.19
FeO	0.2	0	0.13	0.08	0.14	0.13
CaO	8.09	8.68	8.35	6.51	6.72	8.24
Na_2O	7.12	6.66	7.03	8.03	7.72	6.75
K_2O	0	0.04	0.07	0.05	0.09	0.07
Total	99.74	99.02	100.36	100.19	101.47	101.28
Oxygen#	8	8	8	8	8	8
Si	2.59	2.57	2.58	2.68	2.63	2.55
Al	1.40	1.43	1.41	1.32	1.39	1.47
Fe	0.01	0	0.01	0.01	0.01	0.01
Ca	0.39	0.42	0.31	0.31	0.32	0.39
Na	0.62	0.58	0.61	0.69	0.65	0.57
K	0	0.01	0.01	0.01	0.01	0.01
Ab	61.43	58	60.15	68.87	67.2	59.5
An	38.57	41.8	39.5	30.9	32.4	40.12
Or	0	0.2	0.35	0.23	0.4	0.38

Table 4. Geochemical compositions of the Golpayegan amphibolites in the Golpaegan metamorphic complex

Components	*a*'-location			*b*'-location			*c*'-location	
	S323	SFG1	SAD1	S447	S2FG2	SFG14	S430	S2FG1
SiO_2	50.79	51.81	49.59	51.15	51.57	53.21	52.3	52.68
Al_2O_3	13.71	13.5	14.67	14.91	14.47	13.85	15.98	13.9
Fe_2O_3	11.24	11.34	10.23	11.93	9.76	11.04	9.31	8.75
MgO	6.98	6.99	7.34	9.4	7.27	7.31	8.7	9.56
CaO	9.52	8.93	10.87	5.4	9.38	8.4	9.1	9.62
Na_2O	3.5	3.5	3.08	3.78	3.14	2.92	2.1	2.12
K_2O	0.4	0.50	0.42	0.15	0.91	0.33	0.55	0.26
MnO	0.21	0.18	0.14	0.22	0.17	0.25	0.12	0.13
TiO_2	1.89	2.19	2.28	2.03	1.14	1.63	0.44	0.82
P_2O_5	0.20	0.20	0.18	0.32	0.16	0.17	0.04	0.02
Cr_2O_3	0.02	0.02	0.03	0.01	0.01	0.03	0.02	0.07
LOI	1.2	1.1	1.08	0.93	1.05	0.93	1.3	1.45
Ba	59	247	1.1	126	419	65	87	39
Ce	22	21	22	45	22	20	15	6
Cs	0.5	0.5	0.5	0.5	0.9	0.5	1	0.5
Dy	9.3	7.19	8.18	10.26	4.29	5.51	2.13	2.26
Er	5.93	4.89	5.13	7.06	2.69	3.57	1.27	1.57
Eu	2.53	1.99	2.08	2.65	1.3	1.56	0.82	0.95
Gd	7.4	5.83	6.51	9.4	3.13	4.6	0.88	0.95
La	10	10	10	21	9	10	7	3
Lu	0.88	0.69	0.72	0.93	0.37	0.51	0.16	0.23
Nb	2.9	3.4	6.1	1	3.8	5.2	21.4	1
Nd	16.5	13.1	15.2	29.3	10.6	11.8	3.3	0.5
Ni	64	56	63	24	25	57	56	98
P	875	890	702	1404	717	746	192	96
Pb	18	36	18	20	20	22	15	11
Pr	3.03	2.28	2.82	6.02	2.03	2.25	0.57	0.06
Rb	17	19	7	12	43	16	26	15
Sm	6.3	4.89	4.64	8.55	3.41	4.05	1.29	1.13
Sr	125.1	151	188	123.6	239	113	143.8	183.2
Tb	1.3	1.08	1.14	1.54	0.66	0.9	0.37	0.39
Th	0.1	0.1	0.1	3.05	0.1	0.45	0.25	0.1
Ti	11325	13137	10835	12147	6830	9805	2643	4916
Tm	0.9	0.68	0.71	0.96	0.41	0.53	0.21	0.27
U	0.3	0.2	0.2	0.6	0.1	0.55	0.3	0.1
V	247	282	255	267	251	252	217	208
Y	41.2	38.7	43.4	52	21.1	28.5	11.3	12.7
Yb	4.7	4.5	4.2	5.7	2.8	3.5	1.7	1.9
Zr	125	135	133	139	124	122	41	52

Major elements (wt %); trace elements (ppm).

Table 5. Rb–Sr and Sm–Nd isotope from the amphibolite in the GMC

Standard Values	SRM 987:	$^{87}Sr/^{86}Sr = 0.710265 \pm 19$ (conf. lim95%, $N = 11$)
	Nd Jndi:	$^{143}Nd/^{144}Nd = 0.5120958 \pm 88$ (conf. lim95%, $N = 12$)

System Rb/Sr

Ref Lab	Ref sample	Litology	Analysis Conc	ppm Sr	ppm Rb	$^{87}Rb/^{86}Sr$	error(2s)	$^{87}Sr/^{86}Sr$	error(2s)
15.28	323	Amphibolite	ICPMS	148	6	0.117	0.006	0.711938	0.000028
15.29	430	Amphibolite	ICPMS	172	4	0.067	0.004	0.708450	0.000028
15.30	447	Amphibolite	ICPMS	144	2	0.040	0.002	0.714986	0.000026

System Sm/Nd

Ref Lab	Ref sample	Litology	Analysis Conc	ppm Nd	ppm Sm	$^{147}Sm/^{144}Nd$	error(2s)	$^{143}Nd/^{144}Nd$	error(2s)
15.28	323	Amphibolite	ICPMS	17.1	5.46	0.193	0.010	0.512697	0.000013
15.29	430	Amphibolite	ICPMS	18.4	4.22	0.139	0.007	0.512352	0.000013
15.30	447	Amphibolite	ICPMS	30.8	8.03	0.158	0.008	0.512652	0.000016

The strain rate (shortening) in the folds was calculated through the following equation:

$$e = (L_2 - L_1)/L_1 \text{ [50]}. \quad (1)$$

The elongation rate was calculated through the following equation:

$$S = L_2/L_1 \text{ [50]}. \quad (2)$$

The L_1 and L_2 are the primary and secondary lengths. The minimum value of shortening was 43% and the maximum was 85% (Table 1). The samples divided into three parts according to the severity of the deformation: moderate, severe and very severe (Table 1).

In the study area, the signatures of shear movement are in the form of sigma and those of extensional-compressional are folded boudinage (Fig. 2b). Shear movement in Golpayegan region displays dextral and sinistral directions (Fig. 2b).

Petrography and Mineral Chemistry in the Amphibolite Rocks

The studied amphibolites in Golpayegan are exposed well at three sampling points in the study region (Fig. 3).

Amphibolites dark-green to black color (Fig. 3a, sample *a*'; Fig. 3b, sample *b*') are associated with granitic gneisses (Neoproterozoic) [37].

Amphibolites green to grey color (Fig. 3c, sample *c*') are associated with granite (Cretaceous), [37] (Fig. 1b).

The Golpayegan amphibolites are formed mainly by oxides and minerals of the next grained sizes (Fig. 4):

— amphibole, plagioclase, minor quartz and sphene (coarse);

— Ti–Fe oxides that display nematoblastic texture (medium);

— amphibole crystals (fine size).

The abundance of plagioclase in amphibolites green to grey color is less than amphibolites dark-green to black color (Figs. 3, 5b, 5c). Orthopyroxene corona is around the amphibole crystals of amphibolites dark-green to black color (Figs. 3a, 3b, 5c).

Based on B (Ca + B$\sum$M2+)/$\sum$B ≥ 0.75 and BCa/B (Ca + Na) ≥ 0.75 ratios [25], amphiboles in the Golpayegan amphibolites are of calcic variety (Table 2). Additionally, the amphiboles are of magnesio-hornblende variety (Fig. 5a, Table 2). Electron microprobe analyses of minerals show that plagioclases are andesine (An 30 to 42%) in chemical composition (Fig. 5b, Table 3).

Whole-Rock Chemistry in the Amphibolite Rocks

For discerning ortho- from para-amphibolite and igneous- from sedimentary-protolith we used geochemical methods besides field and textural properties to determine the provenance of amphibolites.

The Golpayegan amphibolites are divided into two types based on the protolith (Fig. 6):

— ortho-amphibolite (igneous) (Fig. 3a, sample *a*', 3b, sample *b*');

— para-amphibolite (sedimentary) (Fig. 3c, sample *c*').

The Golpayegan ortho-amphibolites fall within the basalt to basaltic andesite field in total alkalis (TA) versus silica diagram by Middlemost [33] and SiO_2 versus Zr/TiO_2 diagram (Fig. 7b) by Winchester and Floyd [73] (Fig. 7a).

Using the Nb/Y–SiO_2 [72] and Y versus Zr diagrams [48] show that all analyzed samples plot within the sub-alkaline and tholeiite to calc-alkaline transition series field (Figs. 7c, 7d).

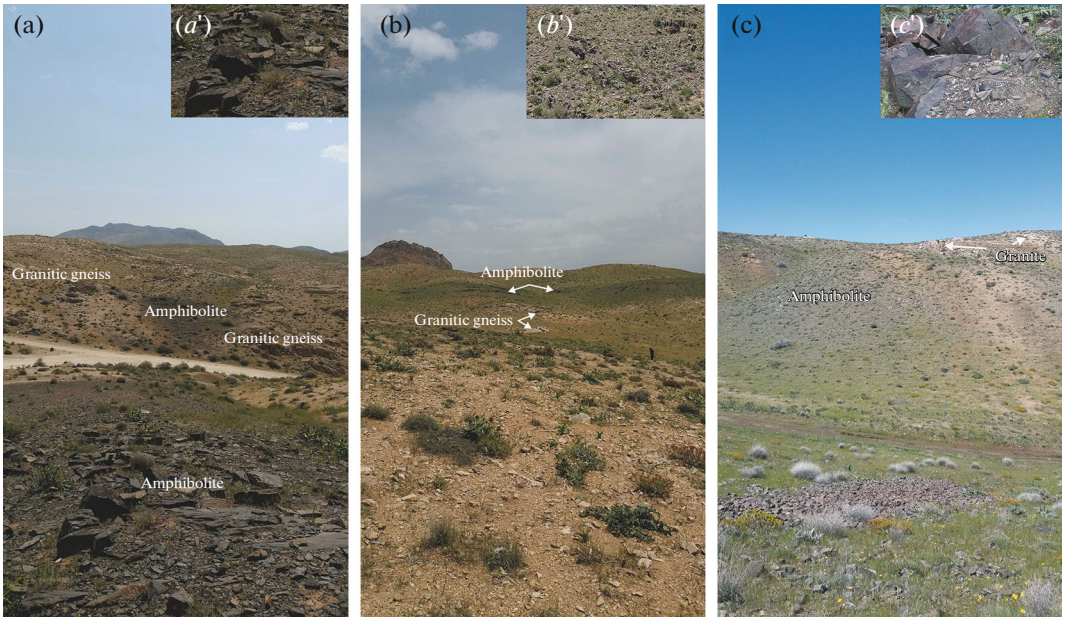

Fig. 3. Photos from the outcrop of amphibolite with granite, schist, and marble in GMC. Dark-green to black amphibolite (sampling point *a*') (a); green to grey amphibolite (sampling point *b*') (b); grey amphibolite (sampling point *c*') (c).

Whole-rock geochemical analyses of samples from ortho-amphibolites of the Golpayegan area show that the SiO_2 content of the analyzed samples is 49.59 to 53.40 (wt %) (Table 4). It shows that they were originally basalt-basaltic andesite in chemical composition. In the studied rocks:

— TiO_2 amount (1.14–2.28 wt %);

— Al_2O_3 amount (13.5–14.911 wt %);

— Fe_2O_3 high values (9.76–11.933 wt %; average: 10/92 wt %);

— K_2O low contents (0.33–0.912 wt %) in the studied rocks conclude their tholeiitic nature.

LOI values of the studied ortho-amphibolites (0.93–1.2 wt %) can be attributed to the presence of hydrous minerals (e.g., amphibole).

Chondrite-normalized REE patterns of the Golpayegan samples show distinct differences in the pattern and amount of trace elements in sampling point *c*' (para-amphibolite) compared to sampling points *b*' and *a*' (ortho- amphibolite) (Figs. 3, 8a). The normalized REE patterns by chondrite of the Golpayegan ortho-amphibolites indicate parallel patterns and slight enrichment in light rare earth elements (LREE) to the heavy rare earth elements (HREE). LREE display more variations than HREE (Fig. 8b). HREE and MREE in the samples show the fairly horizontal trend.

In spider-diagrams of the elements normalized by primitive mantle and normalized by N-MORB, the ortho-amphibolite samples show positive anomalies of LILE (e.g., Rb, Cs, Pb, K and U) and negative anomalies of HFSE (e.g., Ti and Nb) (Figs. 8c, 8d). In the Golpayegan ortho-amphibolites, HFS elements pattern approximates the normal mid-ocean ridge basalts (N-MORB). Also, the pattern of LIL elements approximates island-arc tholeiitic basalts (IATB).

DISCUSSION

The Golpayegan Amphibolites and Protolite

The Golpayegan amphibolites were studied at three sampling points (Figs. 1b; 3):

— *a*' (around Aderba Village);

— *b*' (between Aderba Village and Ochestan Farm);

— *c*' (around Ochestan Farm).

Based on B (Ca + B∑M2+)/∑B ≥ 0.75 and BCa/B (Ca+Na) ≥ 0.75 ratios [25], amphiboles of the Golpayegan are classified as calcic-amphiboles (Table 2).

The Golpayegan amphibolites are similar as per the mineral composition of amphibole and plagioclase but based geochemically, they are different in protolith as per major and trace elements (Figs. 5a, 5b, 6, 8a). They are divided into para-amphibolite located at *c*' sampling point and ortho-amphibolite at *a*' and *b*' sampling points (Figs. 1a, 3).

Sr–Nd Isotopes for Amphibolite Rocks

Thiele et al. [66] suggested the Precambrian age for the metamorphic rocks of Golpayegan region. Based on rock units from Moosavi et al. [37], the studied amphibolites have the Neoproterozoic age (Fig. 1b). Therefore, initial Sr and Nd isotopic ratios of all samples were calculated based on the age of 600 Ma. For the Golpayegan amphibolites, the values of the initial

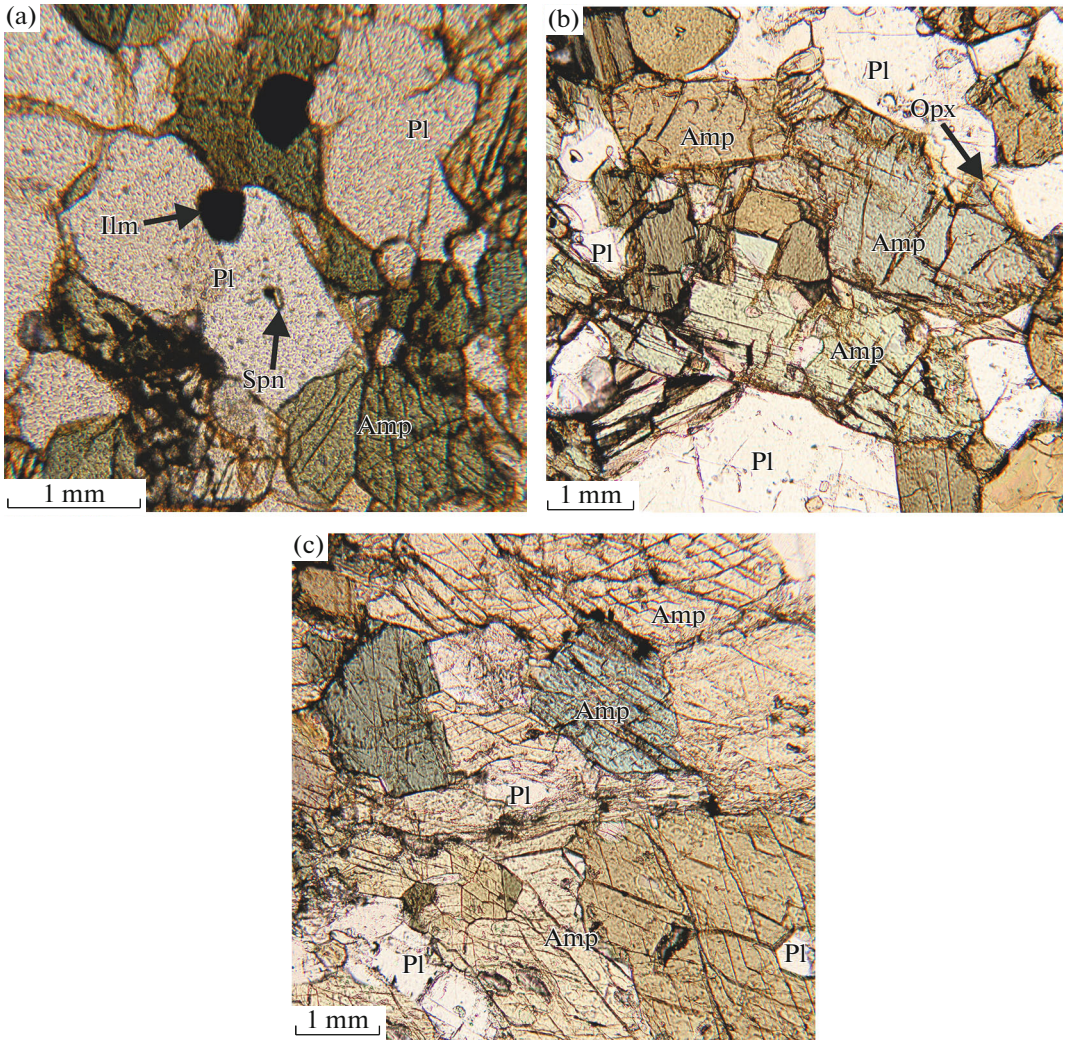

Fig. 4. Photomicrographs of the amphibolite in the GMC. The Golpayegan amphibolites are mostly formed by amphibole and plagioclase and minor ilmenite and sphene (ppl) (a); The orthopyroxene corona is around the amphibole crystals of amphibolite (ppl) from sampling points *a*' and *b*', indicated: amphibole (Amp), plagioclase (Pl), orthopyroxene (Opx), ilmenite (Ilm), sphene (Spn) (b); In amphibolites from sampling point *c*', the amount of plagioclase is less than that of amphibole (ppl) (c).

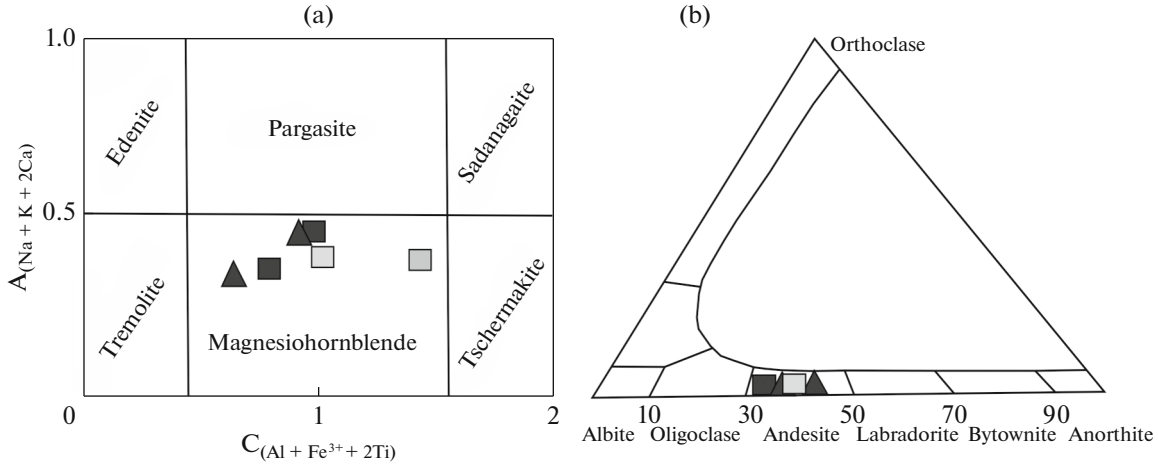

Fig. 5. $^{C}(Al + Fe^{+3} + 2Ti)$ versus $^{A}(Na + K + 2Ca)$ [25] showing the amphibole chemistry (a); Or–Ab–An diagram showing the composition of plagioclases [11], sampling points: *a*' (grey square), *b*' (black square), *c*' (black triangle) (b).

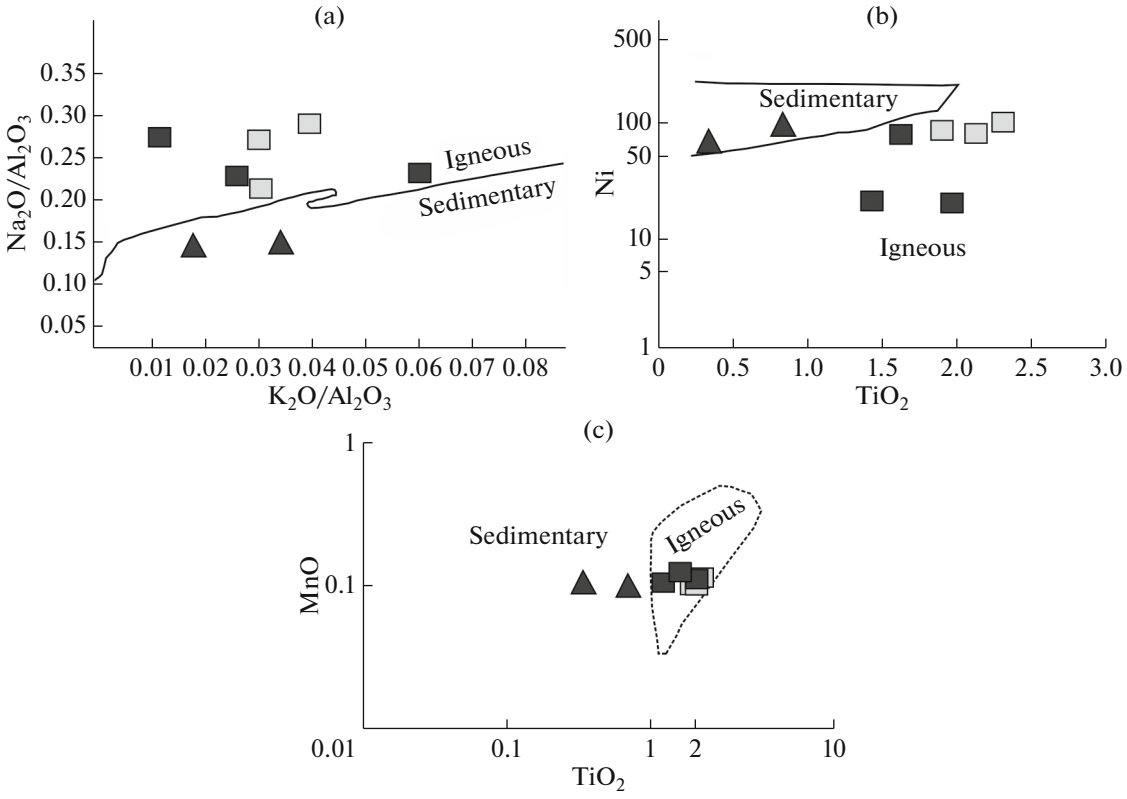

Fig. 6. Protolith discrimination diagrams for the amphibolites from sampling points *a*' (grey square) and *b*' (grey square), K_2O/Al_2O_3 versus Na_2O/Al_2O_3 [17] (a); TiO_2 versus Ni [28] (b); TiO_2 versus MnO [34], sampling point *c*' (black triangle) (c).

$^{87}Sr/^{86}Sr$ isotope ratio are between 0.708450–0.714986, and the initial isotopic ratio of $^{143}Nd/^{144}Nd$ is between 0.512352–0.512697 (Table 5).

The calculated εNd(600 Ma) values for amphibolite rocks (Fig. 3):

+1.44 (sample *a*');

+3.24 (sample *b*');

–1.15 (sample *c*').

Epsilon (ε) values were calculated using present-day ratio of:

— $^{87}Sr/^{86}Sr = 0.7045$ and $^{87}Rb/^{86}Rb = 0.0827$ for the Bulk Silicate Earth (BSE) [12];

— $^{143}Nd/^{144}Nd = 0.512638$ and $^{147}Sm/^{144}Nd = 0.1967$ for the Chondritic Uniform Reservoir (CHUR) [27].

The $^{87}Sr/^{86}Sr$ initial isotopic ratio versus εNd(600 Ma) diagram of the Golpayegan amphibolite samples display variable Sr–Nd isotopic compositions which have strong deviation from the mantle array (Fig. 9). Also, this diagram shows that the protolith of amphibolites in the *c*' sampling point originate from the crust, and the protolith of amphibolites in *a*' and *b*' sampling points originate from the mantle (Figs. 3, 9). The high ratio of initial $^{87}Sr/^{86}Sr$ in ortho-amphibolites can be due to the isotopic exchange resulted from hydrothermal alteration of seawater [13, 44] (Table 5; Fig. 9).

Petrogenesis and Tectonic Setting of Ortho-Amphibolites

The Golpayegan ortho-amphibolites (*a*' and *b*' sampling points) have derived from the mantle origin as per the petrographic and geochemical similarities and have been affected by identical post-magmatism events (Figs. 3a, 3b).

Chondrite-normalized REE patterns show enrichment in LREE and an almost flat HREE pattern (Figs. 8a, 8b). In the chondrite-normalized REE diagram of the Golpayegan ortho- amphibolites, the positive Eu anomaly has been a reason for the insignificance of plagioclase fractionation and the flat pattern in HREE and LREE enrichment indicates the absence of garnet in the mantle source because HREE is compatible in garnet structure and has high garnet/melt partition coefficients [52] (Fig. 8b).

The REE ratios (chondrite normalized) of the Golpayegan ortho-amphibolites are $(La_N/Yb_N) = 1.42–2.90$, $(Sm_N/Yb_N) = 1.17–2.62$ and $(Gd_N/Yb_N) = 0.86–1.31$, which the low values of these ratios indicate low separation of HREE and partial melting of the mantle originated from the spinel stability field [30, 32]. The ortho-amphibolites in the study area are

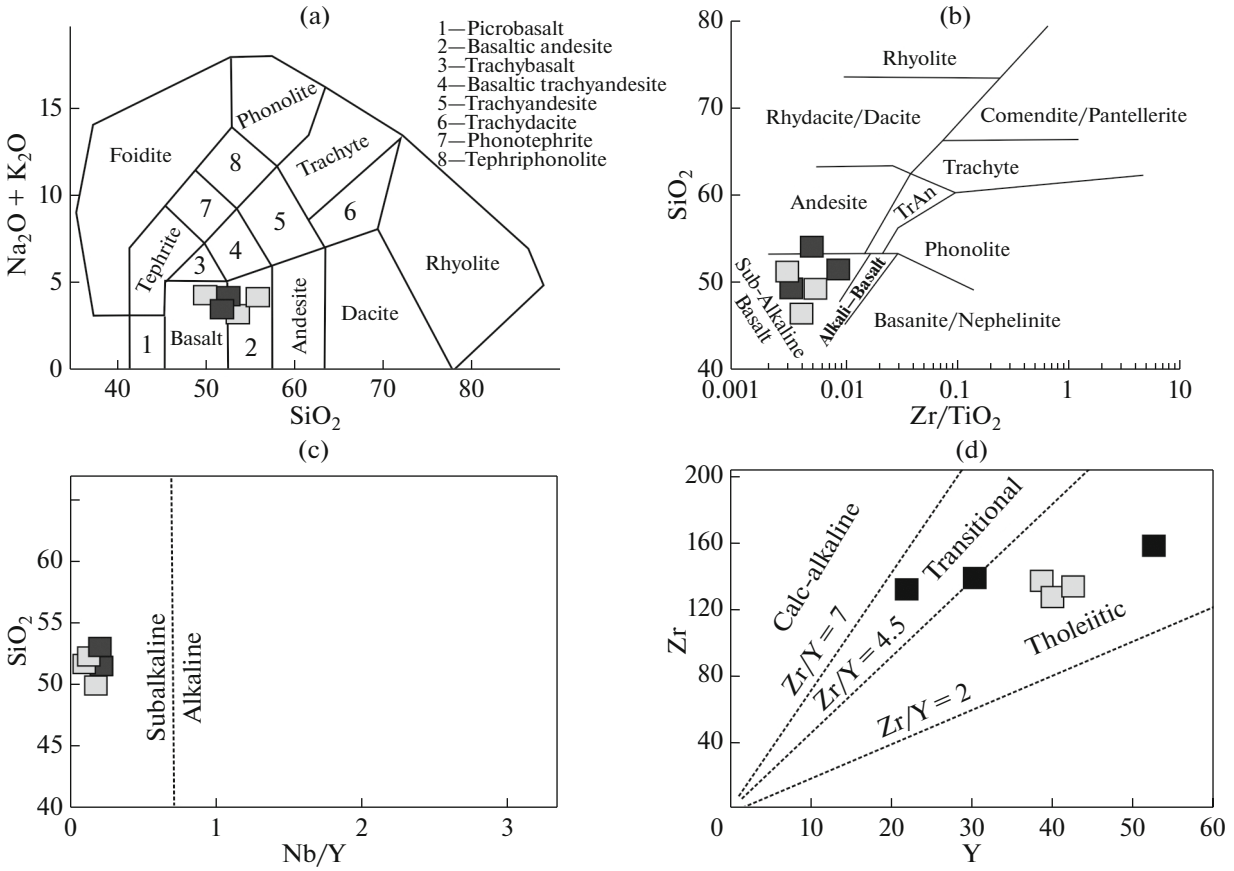

Fig. 7. Classification diagrams (a)–(b) and discrimination diagram (c)–(d) for the Golpayegan ortho-amphibolites. SiO_2 versus $Na_2O + K_2O$ [33] (a); SiO_2 versus Zr/TiO_2 [73] (b); Nb/Y versus SiO_2 [72] (c); Y versus Zr [48] (d). Sampling points: *a*' (grey square), *b*' (black square).

of MORB type of generated magma and continental plate margin basalts (Fig. 10). In the La versus La/Sm diagram, the Golpayegan ortho-amphibolite samples were formed through partial melting of the mantle in the spinel stability field, indicating 8–20% of the partial melting of the E-MORB source [4] (Fig. 11a).

The primitive mantle-normalized and N-MORB-normalized spider diagrams show positive anomalies for Rb, Cs, Pb, K, and U and negative anomalies for Nb, Th, and Ti (Figs. 8c, 8d). The depletion in Nb and enrichment in the LILE (such as Cs and U), LREE, and Pb may be due to magmas originating from an enriched mantle (by the fluid) or to crustal contamination of magma's originating from the mantle [29, 76].

In the $^{147}Sm/^{144}Nd$ versus εNd (600 Ma) diagram [68] (Fig. 11b), the Golpayegan ortho-amphibolites (*a*' and *b*' sampling points) fall within the E-MORB field (Figs. 3a, 3b). The back-arc basin for tectonic setting is suggested of the ortho-amphibolite samples (Fig. 12). In the Golpayegan ortho-amphibolites, the HFS elements' pattern is similar to N-MORB (negative anomalies of HFSE) and the LIL elements' pattern is similar to IATB (positive anomalies of LILE), which this is of magma properties in the back-arc basin [53] (Figs. 8c, 8d). In the back-arc basin, basalts (ortho-amphibolites) are essentially from 6 to 30 times further enriched in chondrites for rare earth elements with usually positive Eu anomaly such as rock samples from *a*' and *b*' sampling points [72] (Figs. 3a, 3b, 8b). Extensional processes in the back-arc basins are similar to those of MORB and are effective by factors such as mantle, oceanic crustal subduction, melting, assimilation, and crystallization [47, 53].

Deformation and Exhumation

In Golpayegan region, shear, extensional-compressional, and compressional movements have generated plastic and brittle deformations on the rocks. The deformations are in the format structures like sigma, boudinage, folded boudinage, and fold (Fig. 2). Over two folding phases have occurred in the GMC (Table 1; Fig. 2). High structural diversity in these folds is one of the most important factors in the complexity of Golpayegan region. The change of folds geometric elements at short distances indicates the influence of multiple stages of evolution on these folds, connoting long and eclectic history.

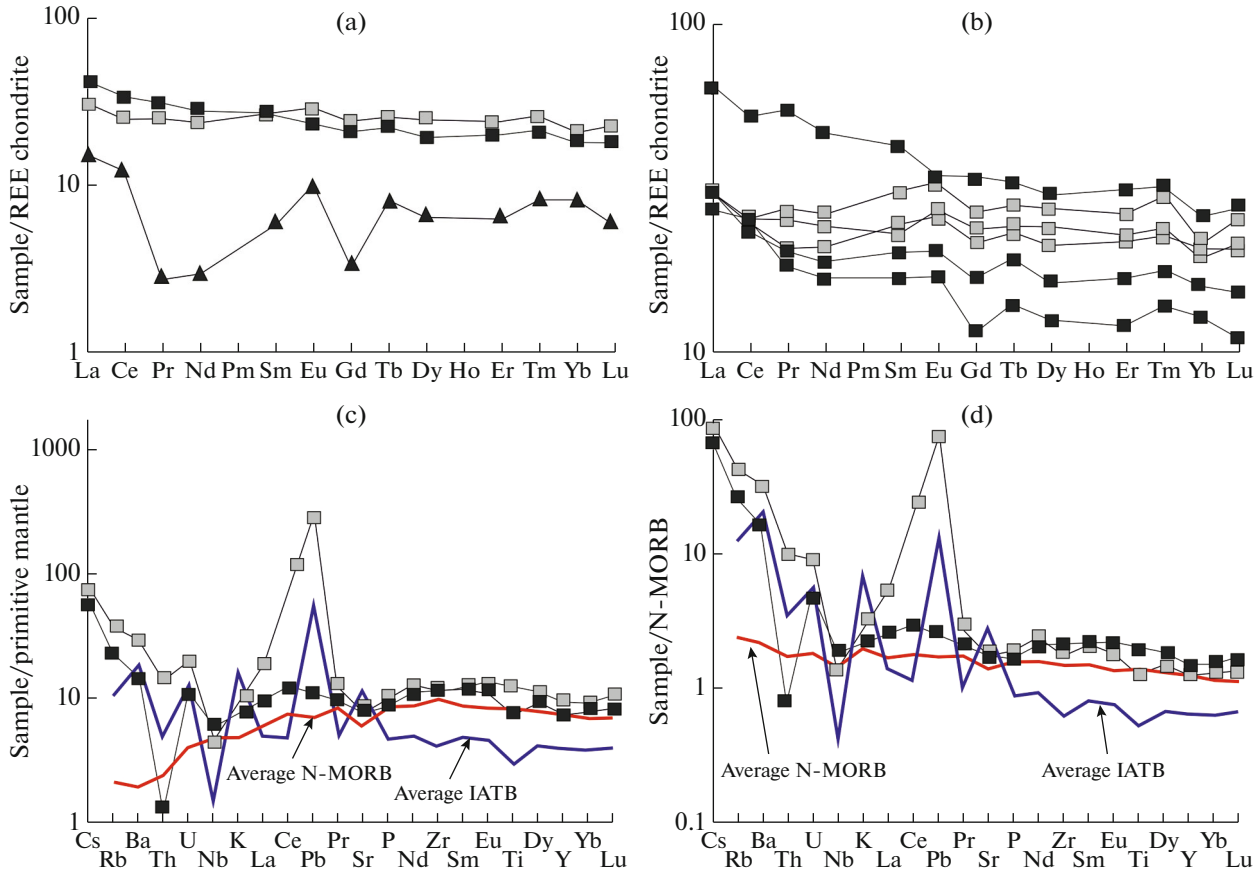

Fig. 8. Chondrite-normalized REE diagram of the Golpayegan amphibolites (a); Chondrite-normalized REE diagram for the Golpayegan ortho-amphibolites from sampling points *a*' (grey square), *b*' (black square), REE contents of chondrite (after [42]) (b); Primitive mantle-normalized multi-element variation diagram for the Golpayegan ortho-amphibolites, compositions for the average primitive mantle data (after [63]) (c); N-MORB-normalized spidergram for the Golpayegan ortho-amphibolites, normalized values for N-MORB (after [63]), the average composition of IATB and N-MORB (after [43]) (d).

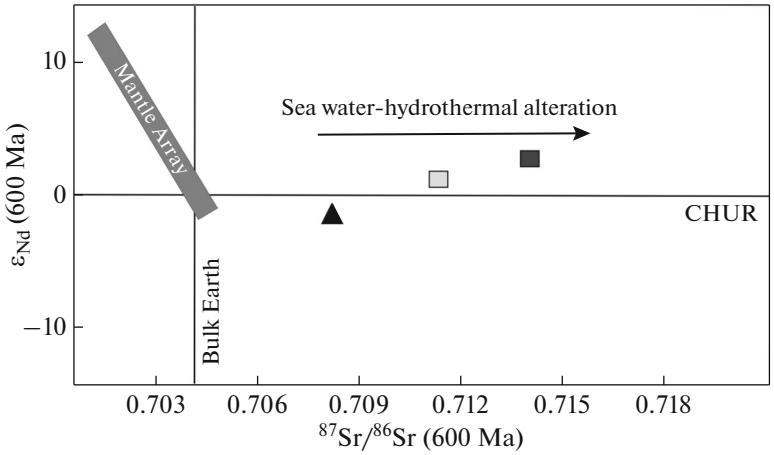

Fig. 9. Plots of initial $^{87}Sr/^{86}Sr$ (t) versus εNd (t) (t = 600 Ma). Indicated sampling points: *a*' (grey square), *b*' (black square), *c*' (black triangle).

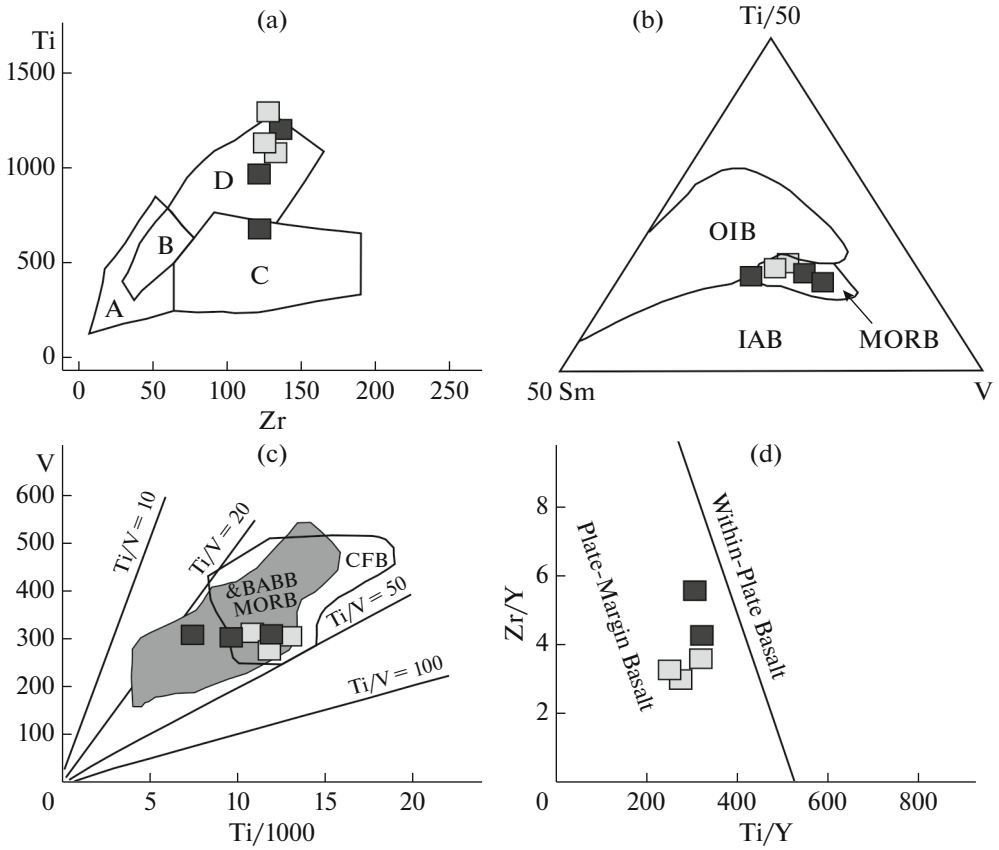

Fig. 10. Geotectonic plots of the Golpayegan ortho- amphibolites. (a) Zr versus Ti [45]. IAT (A), MORB-CAB-IAT (B), CAB (C), MORB (D); (b) Sm*50-Ti/50-V diagram [70]; (c) Ti/1000 versus V [61]; (d) Ti/Y versus Zr/Y [46]. Island-arc tholeits (IAT), island arc basalts (IAB), back-arc basin basalts (BABB), continental flood basalts (CFB), mid-ocean ridge basalts (MORB), oceanic island basalts (OIB), calc-alkaline basalts (CAB). Indicated sampling points: *a*' (grey square), *b*' (black square).

Measuring (shortening) strain shows that the main factor in the formation of interfering fold patterns in Golpayegan region may is strain variations due to varied orogeny phases (Table 1).

The severity of the plastic deformation in the folds indicates that these rocks have deformed in the deep portions of the Earth crust. Then, they had exposed at the surface or uplifted until near the surface during some tensional movements and exhumation [41]. These rocks are old (Neoproterozoic age [37]) and were deformed during the Neoproterozoic orogenic phases, then they were affected by subsequent phases, either. Due to the recent strike-slip movements, this tectonic unit had sheared horizontally similar to a card box [40].

Back-Arc Basin in Sanandaj–Sirjan Zone

The samples are from Golpayegan metamorphic complex at Sanandaj–Sirjan zone as a part of Zagros orogeny, which itself is a part of the Alpine–Himalayan orogenic belt [1, 7]. It is related to the tectonic phases associated with the opening and closure of the Neo-Tethyan Ocean during the Mesozoic [14, 24]. In Sanandaj–Sirjan, the back-arc basin was formed in two different periods. The first back-arc basin was formed in the Peri-Gondwana at 570 Ma. This is related to the Cadomian magmatism in various regions of Iran such as SSZ [57]. The entire Cadomian crust including Iran has separated from Gondwana during Permian–Triassic time and rested adjacent to the southern side of Eurasia [57]. The second back-arc basin existed in the Late Triassic–Early Jurassic in the area located between Central Iran and Sanandaj–Sirjan zone [2, 18, 19, 58].

Based on the age of the Golpayegan ortho-amphibolites (Late Neoproterozoic [37]), these rocks correspond with the Cadomian back-arc in the Peri-Gondwana's north. The Cadomian igneous and metamorphic rocks comprise most of the basement of Iran [57]. According to Linnemann et al. [31], the evolution of peri-Gondwana during Ediacaran–Cadomian is based on the arc-back- arc basin model. Golpayegan ortho-amphibolites (i.e., basalt-andesitic basalt of tholeiitic composition pertaining to the Cadomian back-arc) were associated with granitic gneiss of protolith age (557 ± 12 Ma) pertaining to the differentiated granites of I-type and of sub-alkaline composition pertaining

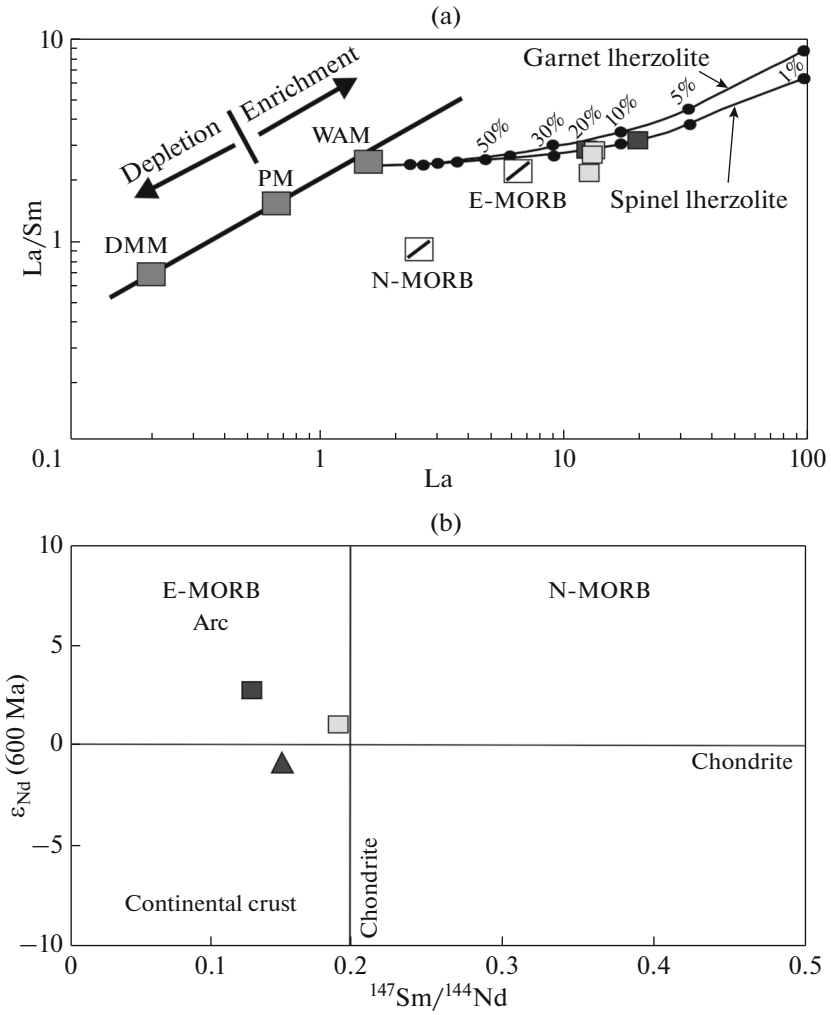

Fig. 11. Plots of La/Sm versus La [4]. DMM (depleted MORB mantle), PM (primitive mantle), WAM (Western Anatolian mantle) (a); Isotopic compositions are plotted in εNd(600 Ma) versus $^{147}Sm/^{144}Nd$ diagram [68] (b). Indicated sampling points: *a*' (grey square), *b*' (black square), *c*' (black triangle).

to Cadomian arc [38], which can be an evidence of the back-arc basin model (Figs. 1b, 4a, 4b).

Cadomian terranes in Iran and Turkey are fragments rifted away from the Arabian–Nubian shield in which the Neoproterozoic crust dominates [21, 57]. Gürsu and Göncüoglu [22] postulated three-stage model for the Cadomian Arc in Turkey, in which arc magmas were injected into the Gondwana basement above the subduction to the south at the northern margin of Gondwana (590–570 Ma). Subsequently, the I-type granites was formed at the early stages of extension and rifting in the continental crust of Gondwana (550–540 Ma). The lithosphere thinned and the back-arc extension took place at the peri-cratonic margin above the southward subduction system during the early Cambrian, generating diabasic dykes and spilitic lavas of back-arc chemical properties (540–530 Ma).

In this study, as peridentical tectonic events of Cadmium magmatism in Iran and Turkey as well as field observations and geochemical results obtained in the Golpayegan metamorphic complex (the relationship between ortho-amphibolites in Golpayegan and granitic gneiss in Golpayegan), the three-stage model of Gürsu and Göncüoglu [22] to interpret the formation of these rocks is more acceptable.

In most continental back-arc regions, extensional tectonics had led to the formation of shallow marine basins on the earth's surface where igneous and sedimentary rocks [8]. Therefore, it can be inferred that association and concurrence of ortho-amphibolites with metamorphosed sedimentary rocks such as marble, quartzite, and schist may confirm their formation in a shallow depositional basin (Fig. 1b).

CONCLUSIONS

(1) In Golpayegan region, the signatures of over two deformation phases in folds of different deformation

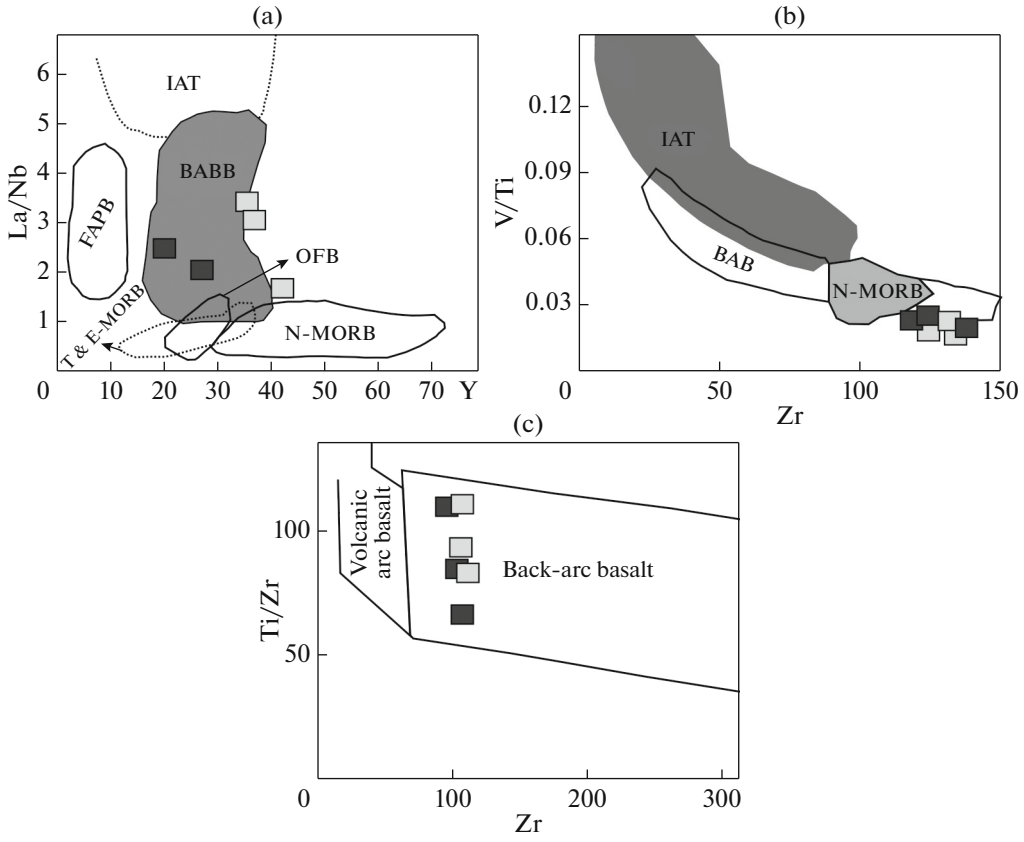

Fig. 12. Determination of back-arc tectonic setting of the Golpayegan ortho-amphibolites. Y versus La/Nb [15]; (b) Zr versus V/Ti [75]; (c) Zr versus Ti/Zr [6] (a); Island-arc tholeits (IAT), fore-arc platform basalts (FAPB), back-arc basin basalts (BABB), oceanic flood basalts (OFB), normal mid-ocean ridge basalts (N-MORB), enriched mid-ocean ridge basalts (E-MORB), transitional mid-ocean ridge basalts (T-MORB). Indicated sampling points: *a*' (grey square), *b*' (black square), *c*' (black triangle).

intensities is evident. Formation of structures such as sigma, boudinage, folded boudinage and fold fabrics due to shear, extensional, extensional-compressional and compressional movements in metamorphic rocks characterize a deep and old setting, which had uplifted through extensional movements and then sheared.

(2) Mineralogically, the Golpayegan amphibolites are similar, while geochemically, they are different in protolith (as per major and trace elements) and are divided into ortho-amphibolite (*a*' and *b*' sampling points) and para-amphibolite (*c*' sampling point). The concentration of εNd(600 Ma) for amphibolitic rocks in *a*', *b*' and *c*' sampling points are +1.44, +3.24, and −1.15, respectively. The Golpayegan ortho-amphibolites are originally tholeiitic basalt-basaltic andesite.

(3) The chemical composition of the ortho-amphibolites is experiencing a transitional between N-MORB (depletion of immobile elements of subduction, e.g., HFSE) and IATB (enrichment of mobile elements of subduction, e.g., LILE) as per the total chemistry of rock, and these rocks belong to the plate-margin setting and basalts of the back-arc basin.

(4) The parental magmas of the Golpayegan ortho-amphibolites have formed by the relatively high degree of partial melting of the spinel lherzolite source. Furthermore, these rocks pertained to the Cadomian back-arc basin in the Peri-Gondwana's north in Neoproterozoic and their generation is similar to back-arc in the Taurides in Turkey.

(5) The occurrence of several ductile and ductile-brittle deformation phases along with the characteristics of deep and old environments as well as the presence of orthoamphibolites with the characteristics of the back arc basin in relation to granite gneiss indicate the default of the Cadomian magmatism in the Golpayegan metamorphic complex.

ACKNOWLEDGMENTS

The authors wish sincerely to acknowledge the Laboratory of Isotope Geology of the University of Aveiro (Portugal) for the Sr and Nd isotopic analysis, and the Department of Geology, University of Isfahan (Iran) for all support provided to this work.

The authors are grateful to anonymous reviewers for helpful comment and thankful to the editor for thorough editing.

FUNDING

The authors thank the University of Isfahan (Iran) for PhD Program financial support in arranging geological field and laboratory works.

CONFLICT OF INTEREST

The authors declare that they have no conflicts of interest.

REFERENCES

1. P. Agard, J. Omrani, L. Jolivet, and F. Mouthereau, "Convergence history across Zagros (Iran): Constraints from collisional and earlier deformation," Int. J. Earth Sci. **94**, 401–419 (2005).
2. M. Ajirlu-Sudi, M. Moazzen, and R. Hajialioghli, "Tectonic evolution of the Zagros Orogen in the realm of the Neotethys between the Central Iran and Arabian Plates: An ophiolite perspective," Central Europ. Geol. **59/x**, 1–27 (2016).
3. M. Alavi, "Sedimentary and structural characteristics of the Paleo-Tethys remnants in northeastern Iran," GSA Bull. **103 (8)**, 983–992 (1991).
4. E. Aldanmaz, J. A. Pearce, M. F. Thirlwall, and J. G. Mitchell, "Petrogenetic evolution of late Cenozoic, post-collision volcanism in Western Anatolia," J. Volcanol. Geotherm. Res. **102**, 67–95 (2000).
5. D. Avigad, T. Weissbrod, A. Gerdes, O. Zlatkin, T. R. Ireland, and N. Morag, "The detrital zircon U–Pb–Hf fingerprint of the northern Arabian–Nubian Shield as reflected by a Late Ediacaran arkosic wedge (Zenifim Formation; subsurface Israel)," Precambrian Res. **266**, 1–11 (2015).
6. L. Bagas, F. P. Bierlein, L. English, J. A. C. Anderson, D. Maidment, and D. L. Huston, "An example of a Palaeoproterozoic back-arc basin: Petrology and geochemistry of the ca. 1864 Ma Stubbins Formation as an aid towards an improved understanding of the Granites Tanamirogen, Western Australia," Precambrian Res. **166**, 168–184 (2008).
7. M. Berberian and G. C. P. King, "Towards a paleogeography and tectonic evolution of Iran," Can. J. Earth Sci. **18**, 210–265 (1981).
8. K. C. Condie, "Geochemistry and tectonic setting of Early Proterozoic supracrustal rocks in the Southwestern United States," J. Geol. **94**, 825–864 (1986).
9. A. Davoudian, J. Genser, F. Neubauer, and N. Shabanian, "$^{40}Ar/^{39}Ar$ mineral ages of eclogites from North Shahrekord in the Sanandaj–Sirjan Zone, Iran: Implications for the tectonic evolution of Zagros orogeny," Gondwana Res. **37**, 216–240 (2016).
10. M. Davoudzadeh and K. Schmidt, "A review of the Mesozoic paleogeography and paleotectonic evolution of Iran," Neues Jahrb. Geol. Palaontol., Abh. **168**, 182–207 (1984).
11. W. A. Deer, R. A. Howie, and J. Zussman, *An Introduction to the Rock-Forming Minerals* (Prentice Hall, Harlow, 1992).
12. D. J. De Paolo, "Trace element and isotopic effects of combined wall rock assimilation and fractional crystallization," Earth Planet. Sci. Lett. **53**, 189–202 (1981).
13. W. M. Fan, Y. J. Wang, A. M. Zhang, F. F. Zhang, and Y. Z. Zhang, "Permian arc–back-arc basin development along the Ailaoshan tectonic zone: Geochemical, isotopic and geochronological evidence from the Mojiang volcanic rocks, Southwest China," Lithos **119**, 553–568 (2010).
14. C. L. Fergusson, P. Nutman, M. Mohajjel, and V. C. Bennett, "The Sanandaj–Sirjan Zone in the Neo-Tethyan suture, western Iran: Zircon U–Pb evidence of late Palaeozoic rifting of northern Gondwana and mid-Jurassic orogenesis," Gondwana Res. **40**, 43–57 (2016).
15. P. A. Floyd, G. Kelling, S. L. GökÇen, and N. GökÇen, "Geochemistry and tectonic environment of basaltic rocks from the Misis ophiolitic mélange, South Turkey," Chem. Geol. **89**, 263–280 (1991).
16. H. Fossen, *Structural Geology* (Cambridge Univ. Press, Cambridge, 2010).
17. R. M. Garrels and F. T. Mackenzie, *Evolution of Sedimentary Rocks* (W. W. Norton &Co, Inc., NY, USA, 1971).
18. A. Ghasemi and C. J. Talbot, "A new tectonic scenario for the Sanandaj–Sirjan Zone (Iran)," Asian Earth Sci. **26**, 683–693 (2006).
19. J. M. Ghazi, M. Mozzen, M. Rahgoshay, and H. Shafaii Moghadam, "Geochemical characteristics of basaltic rocks from the Nain ophiolite (Central Iran); constraints on mantle wedge source evolution in an oceanic back arc basin and a geodynamical model," Tectonophysics **574–575**, 92–104 (2012).
20. D. Grujic, "The influence of initial fold geometry on Type-1 and Type-2 interference patterns: An experimental approach," J. Struct. Geol. **15**, 293–307 (1993).
21. S. Gürsu, "A new petrogenetic model for meta-granitic rocks in the central and southern Menderes Massif–W Turkey: Implications for Cadomian crustal evolution within the Pan-African mega-cycle," Precambrian Res. **275**, 450–470 (2016).
22. S. Gürsu and M. C. Göncüoglu, "Early Cambrian back-arc volcanism in the Western Taurides, Turkey: Implications for the rifting along northern Gondwanan margin," Geol. Mag. **142 (5)**, 617–631(2005).
23. J. Hassanzadeh, D. F. Stockli, B. K. Horton, G. J. Axen, L. D. Stockli, M. Grove, A. K. Schmitt, and J. D. Walker, "U–Pb zircon geochronology of late Neoproterozoic–Early Cambrian granitoids in Iran: Implications for paleogeography, magmatism, and exhumation history of Iranian basement," Tectonophysics **451**, 71–96 (2008).
24. J. Hassanzadeh and B. P. Wernicke, "The Neotethyan Sanandaj–Sirjan zone of Iran as an archetype for passive margin-arc transitions," Tectonics **35**, 586–621 (2016).
25. F. C. Hawthorne, R. E. Oberti, G. V. Harlow, W. F. Maresch, R. C. Martin, J. C. Schumacher, and M. D. Welch, "Nomenclature of the amphibole supergroup," Am. Mineral. **97**, 2031–2048 (2012).
26. O. Hemmati, S. M. Tabatabaei Manesh, and A. R. Nadimi, "Deformation mechanisms of Darreh Sary metapelites, Sanandaj–Sirjan Zone, Iran," Geotectonics **52**, 281–296 (2018).

27. S. B. Jacobsen, G. J. Wasserburg, "Sm and Nd isotopic evolution of chondrites," Earth Planet. Sci. Lett. **50**, 139–150 (1980).

28. K. Kocak, H. Kurt, Z. Veysel, and E. C. Ferré, "Characteristics of the amphibolites from Nigde metamorphics (Central Turkey), deduced from whole rock and mineral chemistry," Geochem. J. **41**, 241–257 (2007).

29. H. Kurt, K. Asan, and G. Ruffet, "The relationship between collision-related calcalkaline, and within-plate alkaline volcanism in the Karacadağ Area (Konya, Central Anatolia)," Geochemistry **68**, 155–176 (2008).

30. S. Lai, J. Qin, Y. Li, S. Li, and M. Santosh, "Permian high Ti/Y basalts from the eastern part of the Emeishan Large Igneous Province, southwestern China: Petrogenesis and tectonic implications," Asian Earth Sci. **47**, 216–230 (2012).

31. U. Linnemann, A. Gerdes, M. Hofmann, and L. Marko, "The Cadomian Orogen: Neoproterozoic to Early Cambrian crustal growth and orogenic zoning along the periphery of the West African Craton—Constraints from U–Pb zircon ages and Hf isotopes (Schwarzburg antiform, Germany)," Precambrian Res. **244**, 236–278 (2014).

32. C. Manikyamba, S. Ganguly, M. Santosh, A. Saha, and G. Lakshminarayana, "Geochemistry and petrogenesis of Rajahmundry trap basalts of Krishna–Godavari Basin, India," Geosci. Front. **6**, 1–15 (2014).

33. E. A. K. Middlemost, "Naming materials in the magma/igneous rock system," Earth Sci. Rev. **37**, 215–224 (1994).

34. S. N. Misra, "Chemical distinction of high-grade ortho- and para-metabasites," Nor. Geol. Tidsskr. **51**, 311–316 (1971).

35. M. Mohajjel and C. L. Fergusson, "Jurassic to Cenozoic tectonics of the Zagros Orogen in northwestern Iran," Int. Geol. Rev. **56**, 263–287 (2014).

36. M. Mohajjel, C. Fergusson, and M. R. Sahandi, "Cretaceous–Tertiary convergence and continental collision, Sanandaj–Sirjan zone, western Iran," Asian Earth Sci. **21**, 397–412 (2003).

37. E. Moosavi, M. Mohajjel, and N. Rashidnejad–Omran, "Systematic changes in orientation of linear mylonitic fabrics: An example of strain partitioning during transpressional deformation in North Golpaygan, Sanandaj–Sirjan zone, Iran," Asian Earth Sci. **94**, 55–67 (2014).

38. A. Moradi, N. Shabanian, A. R. Davoudian, A. Hossein Azizi, J. F. Santos, and Y. Asahara, "Geochronology and petrogenesis of the Late Neoproterozoic granitic gneisses of Golpayegan metamorphic complex: a new respect for Cadomian crust in the Sanandaj–Sirjan zone, Iran," Int. Geol. Rev. **64** (2020). https://doi.org/10.1080/00206814.2020.1821251

39. A. Nadimi, "Structural analysis of the Hasan-Robat marbles as traces of folded basement in the Sanandaj–Sirjan Zone, Iran," Geotectonics **49** (6) 560–578 (2015).

40. A. Nadimi and A. Konon, "Strike-slip faulting in the central part of the Sanandaj–Sirjan Zone, Zagros Orogen, Iran," J. Struct. Geol. **40**, 2–16 (2012).

41. A. Nadimi and H. Nadimi, "Exhumation of old rocks during the Zagros collision in the northwestern part of Zagros Mountains, Iran," GSA Bull. **444**, 105–122 (2008).

42. N. Nakamura, "Determination of REE, Ba, Fe, Mg, Na and K in carbonaceous and ordinary chondrites," Geochim. Cosmochim. Acta **38**, 757–775 (1974).

43. Y. Niu and M. J. O'Hara, "Origin of ocean island basalts: A new perspective from petrology, geochemistry, and mineral physics considerations," Geophys. Res. **108** (B4), (2003).

44. R. K. O'Nions, S. R. Carter, R. S. Cohen, N. M. Evensen, and P. J. Hamilton, "Pb, Nd and Sr isotopes in oceanic ferromanganese deposits and ocean floor basalts," Nature **273**, 435–438 (1978).

45. J. A. Pearce and J. R. Can, "Tectonic setting of basic volcanic rock determined using Trace Element Analyses," Earth Planetary Sci. Lett. **19**, 290–300 (1973).

46. J. A. Pearce and G. H. Gale, "Identification of ore-deposition environment from trace-element geochemistry of associated igneous host rocks," Spec. Publ.—Geol. Soc. London **7**, 14–24 (1977).

47. J. A. Pearce, and R. J. Stern, "Origin of back-arc basin magmas: Trace element and isotopic perspectives," in *Back-Arc Spreading Systems: Geological, Biological, Chemical, and Physical Interactions*, Ed. by D. M. Christie, C. R. Fisher, S. M. Lee, and S. Givens (Geophys. Monogr. Ser., AGU. 2006), pp. 63–86.

48. S. J. Piercey, D. C. Murphy, J. K. Mortensen, and R. A. Creaser, "Mid-Paleozoic initiation of the northern Cordilleran marginal back-arc basin: Geologic, geochemical, and neodymium isotope evidence from the oldest mafic magmatic rocks in the Yukon–Tanana terrane, Finlayson Lake district, southeast Yukon, Canada," GSA Bull. **116**, 1087–1106 (2004).

49. N. Rachidnejad-Omran, M. Hachem Emami, M. Sabzehei, E. Rastad, H. Bellon, and A. Piqué, "Lithostratigraphie et histoire paléozoïque à paléocène des complexes métamorphiques de la région deMuteh, zone de Sanandaj-Sirjan (Iran méridional)," C. R. Geosci. **334**, 1185–1191 (2002).

50. J. G. Ramsay, *Folding and Fracturing of Rocks* (McGraw Hill, NY, USA, 1967).

51. J. G. Ramsay and M. Huber, *The Techniques of Modern Structural Geology,* Vol. 2*: Folds and Fractures* (Pergamon Press, London, UK, 1987).

52. H. R. Rollinson, *Using Geochemical Data: Evolution, Presentation, Interpretation* (Longman Sci. Techn., London, UK, 1993).

53. A. D. Saunders and J. Tarney, "Geochemical characteristics of basaltic volcanism within back-arc basins," Spec. Publ.—Geol. Soc. London **16**, 59–76 (1984).

54. J. C. Schumacher, "The estimation of ferric iron in electron microprobe analysis of amphiboles," Mineral. Mag. **61** (405), 312–321 (1997).

55. A. M. C. Şengör, *The Cimmeride Orogenic System and the Tectonics of Eurasia* (GSA Spec. Pap., USA. 1984, Vol. 195).

56. H. Shafaii Moghadam, M. Khademi, Z. Hu, R. J. Stern, J. F. Santos, and Y. Wu, "Cadomian (Ediacaran–Cambrian) arc magmatism in the ChahJam–Biarjmand metamorphic complex (Iran): Magmatism along the northern active margin of Gondwana," Gondwana Res. **27** (1), 439–452 (2015).

57. H. Shafaii Moghadam, X. H. Li, R. J. Stern, J. F. Santos, G. Ghorbani, and M. Pourmohsen, "Age and nature of 560–520 Ma calc-alkaline granitoids of Biarjmand, northeast Iran: Insights into Cadomian arc magmatism in northern Gondwana," Int. Geol. Rev. **58**, 1492–1509 (2016).
58. H. Shafaii Moghadam, H. Whitechurch, M. Rahgoshay, and I. Monsef, "Significance of Nain–Baft ophiolitic belt (Iran): Short-lived, transtensional Cretaceous back-arc oceanic basins over the Tethyan subduction zone," C. R. Geosci. **341**, 1016–1028 (2009).
59. F. Shakerardakania, X. H. Lia, X. X. Ling, J. Lia, G. Q. Tang, Y. Liu, and B. Monfaredi, "Evidence for Archean crust in Iran provided by ca 2.7 Ga zircon xenocrysts within amphibolites from the Sanandaj–Sirjan zone, Zagros orogeny," Precambrian Res. **332**, 1–12 (2019).
60. M. R. Sheikholeslami, M. R. Ghassemi and J. Hassanzadeh, "Tectonic evolution of the hinterland of the Zagros Orogen revealed from the deformation of the Golpaygan Metamorphic Complex, Iran," J. Asian Earth Sci. **182**, 103929 (2019).
61. J. W. Shervais, "Ti–V plots and the petro genesis of modern and ophiolitic lavas," Earth Planet. Sci. Lett. **59**, 101–118 (1982).
62. H. Soffel, M. Davoudzadeh, C. Rolf, and S. Schmidt, "New palaeomagnetic data from Central Iran and the Triassic palaeoreconstruction," Geol. Rundsch., **85**, 293–302 (1996).
63. S. S. Sun and W. F. McDonough, "Chemical and isotopic systematics of oceanic basalts: Implication for mantle composition and processes," in *Magmatism in Oceanic Basins,* Ed. by A. D. Saunders and M. J. Norry (Geol. Soc. London, UK, 1989. Vol. 42), pp. 313–345. https://doi.org/10.1016/0012-821X(79)90013-X
64. G. M. Stampfli, "*Tethyan Oceans*," in *Tectonics and Magmatism in Turkey and the Surrounding Area,* Ed. by E. Bozkurt, J. A. Winchester, and J. D. A. Piper (Spec. Publ.—Geol. Soc. London, 2000. Vol. 173, no. 1), pp. 1–23. https://doi.org/10.1144/GSL.SP.2000.173.01.01
65. M. Takin, "Iranian geology and continental drift in the Middle East," Nature **235**, 147–150 (1972).
66. O. Thiele, M. Alavi-Naini, R. Assefi, A. Hushmand-Zadeh, K. Seyed-Emami, and M. Zahedi, *Explanatory Text of the Golpaygan Quadrangle Map. Scale 1 : 250000* (Geol. Surv. Iran, 1968. Sh. E7).
67. J. E. Tillman, A. Poosti, S. Rossello, and A. Eckert, "Structural evolution of Sanandaj–Sirjan Ranges near Esfahan, Iran," Am. Assoc. Petrol. Geol. Bull. **65**, 674–687 (1981).
68. K. A. Tung, H. Y. Yang, D. Y. Liu, J. X. Zhang, H. J. Yang, Y. H. Shau, and C. Y. Tseng, "The amphibolite-facies metamorphosed mafic rocks from the Maxianshan area, Qilian block, NW China: A record of early Neoproterozoic arc magmatism," Asian Earth Sci. **46**, 177–189 (2012).
69. P. A. Ustaömer, T. Ustaömer, A. Gerdes, A. H. F. Robertson, and A. S. Collins, "Evidence of Precambrian sedimentation/magmatism and Cambrian metamorphism in the Bitlis Massif, SE Turkey utilising whole-rock geochemistry and U–Pb LA-ICP-MS zircon dating," Gondwana Res. **21**, 1001–1018 (2012).
70. P. Vermeesch, "Tectonic discrimination diagrams revisited," Geochem., Geophys., Geosyst. **7**, 1–55 (2006).
71. M. Wang, C. Li, and C. Ming-Xua, "Dating of detrital zircons from the Dabure clastic rocks: The discovery of Neoproterozoic strata in southern Qiangtang, Tibet," Int. Geol. Rev. **58**, 216–227 (2016).
72. M. Wilson, *Igneous Petrogenesis: a Global Tectonic Approach* (Springer, Dordrecht-Netherlands, 1989).
73. J. A. Winchester and P. A. Floyd, "Geochemical discrimination of different magma series and their differentiation products using immobile elements," Chem. Geol. **20**, 325–343 (1977).
74. D. L. Whitney and B. W. Evans, "Abbreviations for names of rock-forming minerals," Am. Mineral. **95**, 185–187 (2010).
75. J. Woodhead, S. Eggins, and J. Gamble, "High field strength and transition element systematics in island-arc and back-arc basin basalts: Evidence for multiphase melt extraction and a depleted mantle wedge," Earth Planet. Sci. Lett. **114**, 491–504 (1993).
76. Y. F. Zheng, "Subduction zone geochemistry," Geosci. Front. **10**, 1223–1254 (2019).